

Dynamically Crosslinked Dry Ion-Conducting Elastomers for Soft Iontronics

Panpan Zhang, Wenbin Guo, Zi Hao Guo, Yuan Ma, Lei Gao, Zifeng Cong, Xue Jiao Zhao, Lijie Qiao, Xiong Pu,* and Zhong Lin Wang*

Soft ionic conductors show great promise in multifunctional iontronic devices, but currently utilized gel materials suffer from liquid leakage or evaporation issues. Here, a dry ion-conducting elastomer with dynamic crosslinking structures is reported. The dynamic crosslinking structures endow it with combined advantageous properties simultaneously, including high ionic conductivity ($2.04 \times 10^{-4} \text{ S cm}^{-1}$ at 25 °C), self-healing capability (96% healing efficiency), stretchability (563%), and transparency (78%). With this ionic conductor as the electrode, two soft iontronic devices (electroluminescent devices and triboelectric nanogenerator tactile sensors) are realized with entirely self-healing and stretchable capabilities. Due to the absence of liquid materials, the dry ion-conducting elastomer shows wide operational temperature range, and the iontronic devices achieve excellent stability. These findings provide a promising strategy to achieve highly conductive and multifunctional soft dry ionic conductors, and demonstrate their great potential in soft iontronics or electronics.

particular, soft iontronics have recently received increasing interests, as the utilization of ion-conducting hydrogels or ionogels endows them characteristics that are hard to be achieved by the counterpart electronics. For example, these quasi-solid-state polymeric ionic conductors are readily stretchable, while most electronic conductors struggle to obtain high stretchability. The electron transfer paths of existing stretchable electronic conductors, such as serpentine-shaped metallic wires and conductive-filler-percolated polymer composites, can be damaged or broken at large strain; while the ion transfer paths along the swollen solvents inside the networks of the gel polymers will not be interrupted at stretched states.^[3] Moreover, polymeric ionic conductors can also easily achieve multiple functions through diverse molecular chain designs,

1. Introduction

Iontronics (or ionotronics) couple the electron/ion charge transfers and exchange signals at the interfaces of electronic/ionic conductors, differentiating them from most electronics using electrons and/or holes as the dominating charge carriers. The concept of iontronics has just been proposed in last decade, despite the fact that the co-transfers of ions and electrons have long been employed in many devices, such as electrochemical energy devices, electrical-double-layer field-effect transistors^[1] and resistance random-access memories.^[2] In

such as transparency, biocompatibility, self-healing capability and biodegradability.^[4,5] Therefore, various multifunctional soft iontronics have been demonstrated using hydrogel/ionogel electrodes, such as artificial muscles^[6,7] and axons,^[8] AC luminescent devices,^[9,10] liquid crystal devices,^[11] touchpads,^[12] and triboelectric nanogenerators.^[3,13]

However, one intrinsic drawback of the current gel electrodes is their low environmental stability and limited operational temperature range. The ionic conductivity and stretchability of hydrogels or organogels can be severely deteriorated due to the dehydration or solvent evaporation at elevated temperature

Dr. P. Zhang, W. Guo, Z. H. Guo, Z. Cong, Dr. X. J. Zhao, Prof. X. Pu, Prof. Z. L. Wang
CAS Center for Excellence in Nanoscience
Beijing Key Laboratory of Micro-Nano Energy and Sensor
Beijing Institute of Nanoenergy and Nanosystems
Chinese Academy of Sciences
Beijing 101400, China
E-mail: puxiong@binn.cas.cn

W. Guo, Z. H. Guo, Z. Cong, Prof. X. Pu, Prof. Z. L. Wang
School of Nanoscience and Technology
University of Chinese Academy of Sciences
Beijing 100049, China

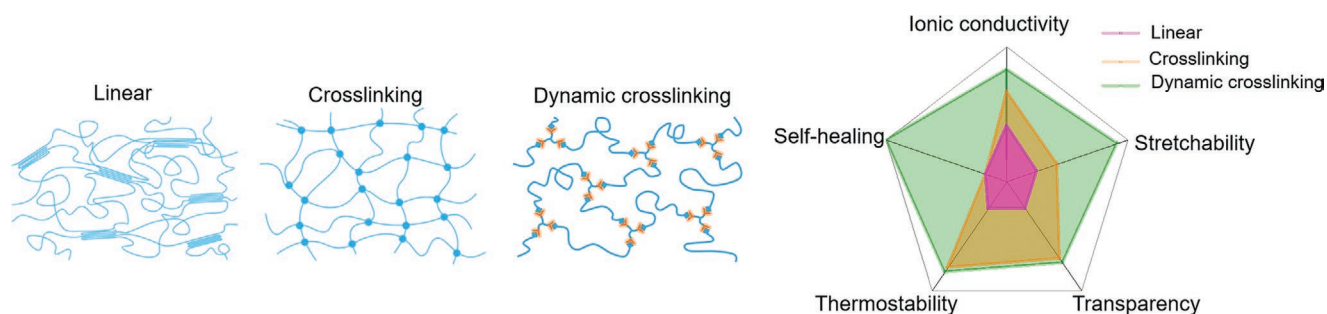
 The ORCID identification number(s) for the author(s) of this article can be found under <https://doi.org/10.1002/adma.202101396>.

DOI: 10.1002/adma.202101396

Y. Ma, Prof. L. Gao, Prof. L. Qiao
Beijing Advanced Innovation Center for Materials Genome Engineering
Institute for Advanced Materials and Technology
University of Science and Technology Beijing
Beijing 100083, China

Prof. X. Pu
Center on Nanoenergy Research
School of Chemistry and Chemical Engineering
School of Physical Science and Technology
Guangxi University
Nanning 530004, China

Prof. Z. L. Wang
School of Materials Science and Engineering
Georgia Institute of Technology
Atlanta, GA 30332-0245, USA
E-mail: zlwang@gatech.edu



Scheme 1. Diagrammatic models of the ion-conducting polymer matrix with linear (L), crosslinking (C), dynamic crosslinking (DC) structures, and the comparison of their important properties.

or after long-time storage at room temperature.^[14,15] Ionogels, though could be nonvolatile, still have the issue of liquid leakage upon deformation. Therefore, liquid-free dry ion-conducting elastomers (ICE) are highly demanded for all-solid-state soft iontronics. However, very limited attempts have recently been carried out to develop dry ICEs for iontronics.^[15–19] “liquid-free” ICEs with self-healing capability has been reported very recently for touch sensors and force sensors.^[17,18] 3D printing capability of ICE has also been demonstrated.^[18] Nevertheless, the utilization of “liquid-free” or dry ICEs in soft iontronics still has not been well explored, and their conductivity should be further improved to compete with gel-based iontronics.

In this work, we design a self-healing, stretchable and transparent poly(ethylene oxide) (PEO)-based dry ICE and demonstrate its application as electrodes in two soft iontronic devices, i.e., iontronic electroluminescent (EL) device and triboelectric nanogenerator (TEG) tactile sensor. The molecular chains of the dry ICE are dynamically crosslinked by reversible imine bonds as described in **Scheme 1**, which reduces its crystallinity, improves the ionic conductivity, and endows the system with self-healing capability and high stretchability. The ionic conductivity is $2.04 \times 10^{-4} \text{ S cm}^{-1}$ at 25 °C, and the ultimate tensile strain reaches 563%. Furthermore, the mechanical and electrical properties can be fully recovered spontaneously upon damages. Lastly, we realize entirely stretchable self-healing EL and TEG devices using the dry ICE electrode and a dielectric elastomer, two devices that are both in sandwich structures but reversed stacking sequences. Due to the absence of liquid molecules, the ICE and corresponding iontronic devices show wide temperature range and excellent stability.

2. Results and Discussion

Dry ion-conducting polymers can typically solvate ions (H^+ , Li^+ , Na^+ , etc.) with heteroatoms (N, S, O, Si, etc.) in the molecular chains, and realize ion transport along or among the chains under bias voltage or concentration gradient.^[20] Generally, ion-conducting polymers with linear chains tend to be semicrystalline, but the ion transfer prefers amorphous regions with activated chain segments or high chain mobility.^[21–23] Strategies such as grafted chain designs, copolymerization or crosslinking are frequently employed to suppress the crystallization of the polymer matrix, so as to improve the ionic conductivity.^[20] Here, we propose to construct dry ICE with dynamic crosslinking

structures, which are expected to bring following advantageous properties (**Scheme 1**).

- 1) Higher ionic conductivity: The crystallinity of the ICE can be suppressed with minimum sacrifice to the chain flexibility. Comparing with strong crosslinking structure, the dynamic crosslinking structure is relative weaker, endowing the networks with even higher chain mobility, as one chain is not “fixed” to one crosslinking point. Instead, the dynamic bond can spontaneously break and re-form crosslinking with other chains. Therefore, better ionic conductivity is expected.
- 2) High stretchability and self-healing capability: The dynamic crosslinking structures would also endow the system elastomeric mechanical behaviors and simultaneously make the ICE self-healable upon damages.
- 3) Excellent thermal stability and potential transparency: There is no obvious melting point (T_m) for crosslinking ICE, which means the stable structure and property in relatively wider temperature range than the semicrystalline counterparts, since drastic property change occurs above melting point. Furthermore, amorphous ICE can also potentially be transparent, unless other opaque additives are utilized.

PEO complexing with lithium salts is an ionic conductor being widely studied as electrolytes in solid-state batteries.^[19,20,24] Linear PEO (L-PEO), due to its semicrystalline structure, shows limited ionic conductivity, low thermal stability and poor stretchability. Crosslinking PEO (C-PEO) has been reported with high stretchability and improved conductivity, but the conductivity still requires further optimization.^[15] Therefore, we designed a dynamic crosslinking PEO (DC-PEO), which was crosslinked by imine bonds as schemed in **Figure 1a**. The imine bond was achieved by a Schiff base reaction between benzene-1,3,5-tricarbaldehyde and amino-terminated poly(ethylene glycol). The Fourier transform infrared spectroscopy (FTIR) confirmed the formation of imine bonds in the DC-PEO (**Figure S1**, Supporting Information). Peaks related to $-(\text{C}=\text{O})-$ and $-\text{C}=\text{N}-$ stretching modes were observed at 1700 and 1646 cm^{-1} , respectively, correspondent to the excessive aldehyde groups and the formed imine bonds in the DC-PEO.^[25] To illustrate the influence of imine-bonded ($\text{C}=\text{N}$) dynamic crosslinking structure on the properties of the ICE, an amine-bonded ($\text{C}-\text{N}$) non-dynamic crosslinking structure ICE was synthesized as the control sample by reducing the $\text{C}=\text{N}$ to $\text{C}-\text{N}$ bond with NaBH_3CN , noted as C-PEO hereafter.

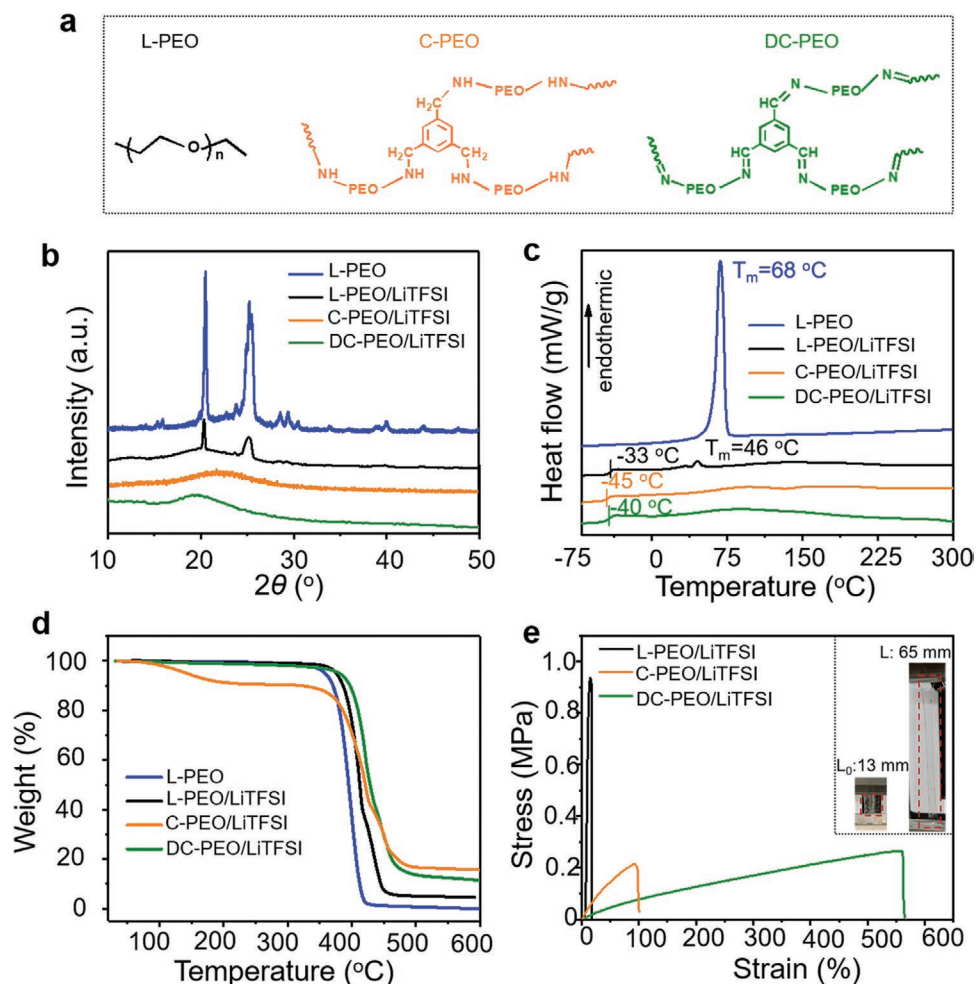


Figure 1. Structures and characterizations of the dynamic crosslinking dry ICE. a) Structures of the L-PEO, C-PEO and DC-PEO. b) XRD, c) DSC and d) TGA of the L-PEO, L-PEO/LiTFSI, C-PEO/LiTFSI, and DC-PEO/LiTFSI. e) The uniaxial tensile stress–strain profiles of L-PEO/LiTFSI, C-PEO/LiTFSI, and DC-PEO/LiTFSI at ambient conditions. The inset photos: the DC-PEO/LiTFSI at initial state and stretched state (strain $\varepsilon = 400\%$).

The FTIR results were confirmed the reduction of imine. Peaks related to $-(N-H)-$ and $-C=N-$ stretching modes were observed at 1578 and 1228 cm^{-1} , respectively (Figure S1, Supporting Information).

The crystallization behaviors were studied by differential scanning calorimetry measurement (DSC) and X-ray diffraction (XRD). Four samples were compared to illustrate the effect of the dynamic crosslinking structure, i.e., a pure L-PEO, a L-PEO/LiTFSI (L-PEO mixed with lithium bis(trifluoromethylsulfonyl)imide), C-PEO/LiTFSI and the DC-PEO/LiTFSI (EO:Li = 8:1 for the three samples). The pure L-PEO exhibits two strong diffraction peaks located at 19.5° and 23.5° (Figure 1b), correspondent to crystal planes of (120) and (032)/(112), respectively.^[26] As for the L-PEO/LiTFSI, these two diffraction peaks can still be clearly observed though the intensity is lowered. Nevertheless, only a broad diffuse peak is observed for the C-PEO/LiTFSI and DC-PEO/LiTFSI, confirming their amorphous structure because of the crosslinking structure. For pure L-PEO, a clear melting peak (T_m : 68°C) is observed from the DSC thermograms (Figure 1c). For the L-PEO/LiTFSI, the melting peak shifts to a lower temperature

(46°C) with significantly suppressed intensity, and a glass-transition temperature (T_g) can be observed at -33°C . In contrast, the C-PEO/LiTFSI and DC-PEO/LiTFSI show no obvious melting peak but a clear glass transition at the T_g of -45 and -40°C , respectively. These results demonstrated that the lithium salts can defect the lattice of PEO molecular chains and lead to the reduced crystallinity.^[27] More importantly, it is strongly supported that the (dynamic) crosslinking structure further leads to the amorphous ion conductor. The thermogravimetric analysis (TGA) confirms that the DC-PEO/LiTFSI is dry and solvent-free, showing almost no weight loss before 300°C (Figure 1d). The degradation temperature of DC-PEO/LiTFSI ($\approx 385^\circ\text{C}$) is slightly higher than that of the L-PEO and L-PEO/LiTFSI because of the crosslinking structure. These thermoanalysis results (DSC and TGA) suggest excellent thermal stability of DC-PEO/LiTFSI.

The DC-PEO/LiTFSI shows an ultimate tensile strength of 262 kPa and a fracture strain of 563% . In contrast, the L-PEO/LiTFSI and C-PEO/LiTFSI only has a fracture strain of $\approx 17.9\%$ and 98.6% , respectively (Figure 1e). The high stretchability of the DC-PEO/LiTFSI is consistent with its amorphous

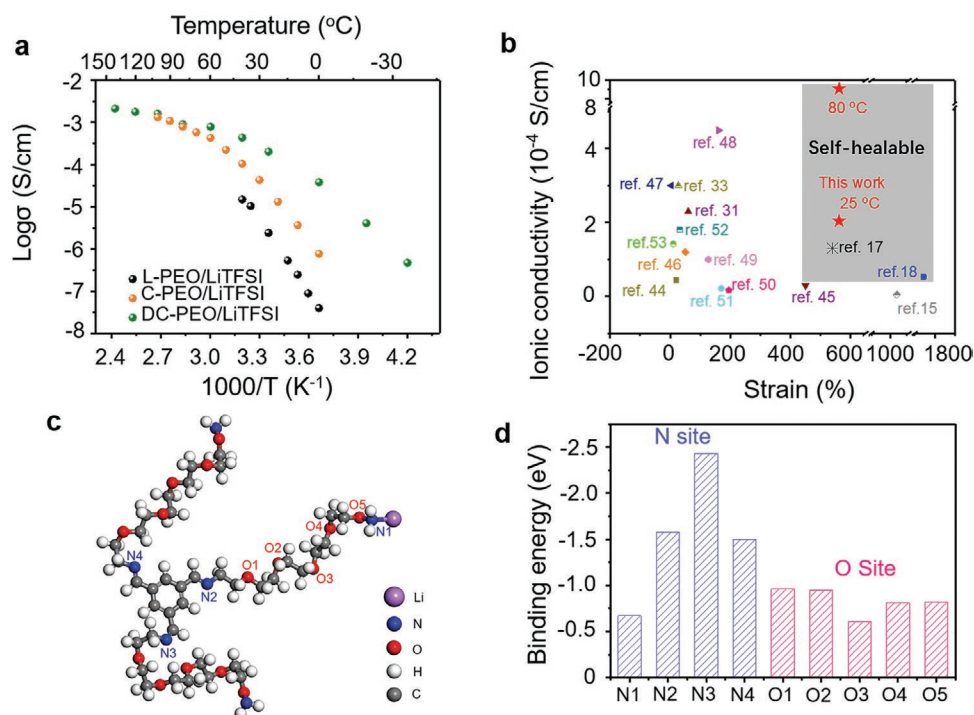


Figure 2. Ion-conducting properties of the DC-PEO/LiTFSI. a) Arrhenius plot of the ionic conductivity of the L-PEO/LiTFSI, C-PEO/LiTFSI and DC-PEO/LiTFSI. b) Comparison of the ionic conductivity, stretchability and self-healing capability of DC-PEO/LiTFSI to other reported ion-conducting polymers: PEGDA/MOF (30 °C);^[44] PI/PEO (30 °C);^[31] VS₅/PEO (25 °C);^[45] xPTHF-SPE (25 °C);^[46] PPC/cellulose (30 °C);^[47] PVA-CN/PAN/SN (25 °C);^[48] HAmCP/PEGDE (30 °C);^[49] PEO/g-C₃N₄ (30 °C);^[50] PEGPEA/SiO₂ (25 °C);^[51] PLiTFSI/PEGM/PEGDMA/EC (30 °C);^[52] EG-P[SSPSiLi-@-MA]/PEO (25 °C);^[53] POSS/PEG (30 °C);^[33] PBA/PEGDA (25 °C);^[15] P(MEA-co-IBA)/LiTFSI (25 °C);^[18] PIL/TFSI (30 °C).^[17] c) The structure of a dynamic crosslinking point used for DFT simulations. d) Adsorbing binding energies of Li ions on N and O sites with different configurations in the molecular chains.

and crosslinking structure discussed above. Cyclic loading-unloading tensile tests were also conducted to the DC-PEO/LiTFSI. Relatively good resilience was obtained when the strain is 100%, but large residual strain was observed after unloading the stress when the strain is higher than 200% (Figure S2, Supporting Information).

The ionic conductivity of the DC-PEO/LiTFSI was then determined by electrochemical impedance spectroscopy (EIS) from -40 to 140 °C, as shown by the Arrhenius plot in Figure 2a. The ionic conductivity of DC-PEO/LiTFSI at 25 °C is 2.04×10^{-4} S cm^{-1} , which is about 2 orders higher than 2.42×10^{-6} S cm^{-1} of the semicrystalline L-PEO/LiTFSI and 1 order higher than 1.33×10^{-5} S cm^{-1} of the C-PEO/LiTFSI (the conductivity of undried L-PEO/LiTFSI with 8.5 wt% residual solvent is 3.9×10^{-5} S cm^{-1} , Figure S3: Supporting Information). Other than the high conductivity, another major advantage of the DC-PEO/LiTFSI is its wide applicable temperature range. When the temperature is as high as 140 °C, the DC-PEO/LiTFSI can still operate and show a conductivity of 2.12×10^{-3} S cm^{-1} ; while the L-PEO/LiTFSI will melt above 46 °C (T_m in Figure 1c). After storing at 140 °C for 7 h in atmosphere environment, the DC-PEO/LiTFSI still showed elastomeric mechanical behaviors, though the stretchability decreased to 383% (Figure S4, Supporting Information). Furthermore, the conductivity of the DC-PEO/LiTFSI at -35 °C can still be measured to be 4.73×10^{-7} S cm^{-1} . The high conductivity and wide operational temperature range of the DC-PEO/LiTFSI are attributed to its amorphous structure and low T_g (-40 °C,

Figure 1c), which imply the high chain mobility and low activation energy (E_a) for ion transfer. The E_a was estimated by fitting the conductivity with Vogel–Tammann–Fulcher (VTF) model (Figure S5, Supporting Information). The E_a of the DC-PEO/LiTFSI is estimated to be 0.388 eV, which is noticeably lower than 1.235 eV of L-PEO/LiTFSI and 1.154 eV for C-PEO/LiTFSI.

The dynamic crosslinking structure of our DC-PEO/LiTFSI has the following two unique characteristics which are beneficial to the ion transportation. Firstly, The N atoms in the imine bonds ($-\text{C}=\text{N}-$) or in the unreacted amino groups ($-\text{NH}_2$) can provide extra sites for solvation of Li^+ ions other than ether oxygen atoms, due to the existence of an electron pair in outermost layer of the N nucleus. Ion transport could also occur between N and O sites or among N sites. The adsorption behaviors of Li^+ on different sites (O and N with different configurations) in DC-PEO/LiTFSI molecule chain was evaluated through the density functional theory (DFT) calculations. PEO chains with five repeated ether oxygen units were simulated for simplification (Figure 2c). The binding energies of the three N sites in imine bonds are -1.58 , -2.43 , and -1.50 eV, respectively, which are even larger than -0.61 to -0.96 eV of the five O sites (Figure 2d), confirming that introduced N atoms help the solvation and transportation of Li^+ ions. Secondly, the chain mobility is higher than PEO crosslinked with strong covalent bonds (C-PEO), as the crosslinking through weak imine bonds are dynamically broken and formed. The significant contribution of the dynamic networks to the conductivity can be strongly supported by comparing the conductivity of the DC-PEO/LiTFSI

and non-dynamic C-PEO/LiTFSI. Meantime, our DC-PEO/LiTFSI also shows higher conductivity than that of other reported crosslinked PEO polymer electrolytes, such as e-beam crosslinked PEO,^[28] crosslinked PEO-g-PEG,^[29] polyethylene crosslinked by PEO,^[30] and PBA crosslinked by PEGDA.^[15]

Figure 2b and Table S1 (Supporting Information) show comprehensive comparisons of our DC-PEO/LiTFSI with some representative reported ether oxide-based ion conductors. The conductivity is generally higher than or comparable with that of PEO with polymer blends,^[15,31,32] PEO with inorganic fillers,^[33–35] Nevertheless, most of these PEO electrolytes are not completely dry and there were possibly residual solvent molecules acting as plasticizers. Furthermore, only very few recent works reported combined excellent elasticity and self-healing capability (will be discussed hereafter).^[17,18]

The self-healing mechanism of DC-PEO/LiTFSI is shown in Figure 3a. Upon damages, imine bonds are broken and hydrolyzed back to aldehyde and amine, which can re-form the imine bonds through a Schiff base reaction between the amino ($-\text{NH}_2$) groups and the $-\text{CHO}$ groups.^[25] Imines react reversibly with water (hydrolysis, which is the reverse process of imine formation), amines (transimination) and preformed imines (metathesis), as depicted in Scheme S1.^[36,37] In our system, the hydrolysis route may be more likely, considering the two facts: excessive amount of aldehydes were used during synthesis and all the experiments were conducted in atmosphere environment. The damages can be then cured automatically. The self-healing property was evaluated by tensile tests

after cutting the DC-PEO/LiTFSI completely into two pieces and healing for different periods of time. The healing efficiency calculated based on the strain to fracture is 94% after 84 h of room-temperature (RT, 20 °C) healing, 80% and 96% after 3 and 6 h healing at 60 °C, respectively (Figure 3b and Figure S7: Supporting Information). For demonstration, a DC-PEO/LiTFSI was cut into two pieces and attached back (Figure 3c-i,ii). After 90 h of autonomous RT healing, the sample can still be stretched for different times (Figure 3c-iii,iv). Optical microscope photos show that a $\approx 150 \mu\text{m}$ wide cleft was healed spontaneously after 48 h in ambient condition (Figure 3c-v,vi). In addition, after being cut completely and healed at 60 °C, the resistance of a DC-PEO/LiTFSI can quickly recover to the original value in ≈ 100 min for each cut (Figure 3d). As for polymer ionic conductors, the ion conduction pathways are fully recovered as long as the molecular chains are healed; while for percolated polymer composites, the electron conduction pathways may not be thoroughly recovered after the healing process.^[25]

In soft iontronic devices, DC-PEO/LiTFSI needs to be connected with metal wires in order to receive electrical stimuli or output electrical signals. It may also be attached with dielectric materials (polyimide (PI), poly(ethylene terephthalate) (PET), etc.). By means of 90°-peeling tests, the peeling forces per width of DC-PEO/LiTFSI on various substrates are shown in Figure S8 (Supporting Information). The DC-PEO/LiTFSI was adhesive to these surfaces which would be favorable for the applications in iontronic devices. The DC-PEO/LiTFSI also

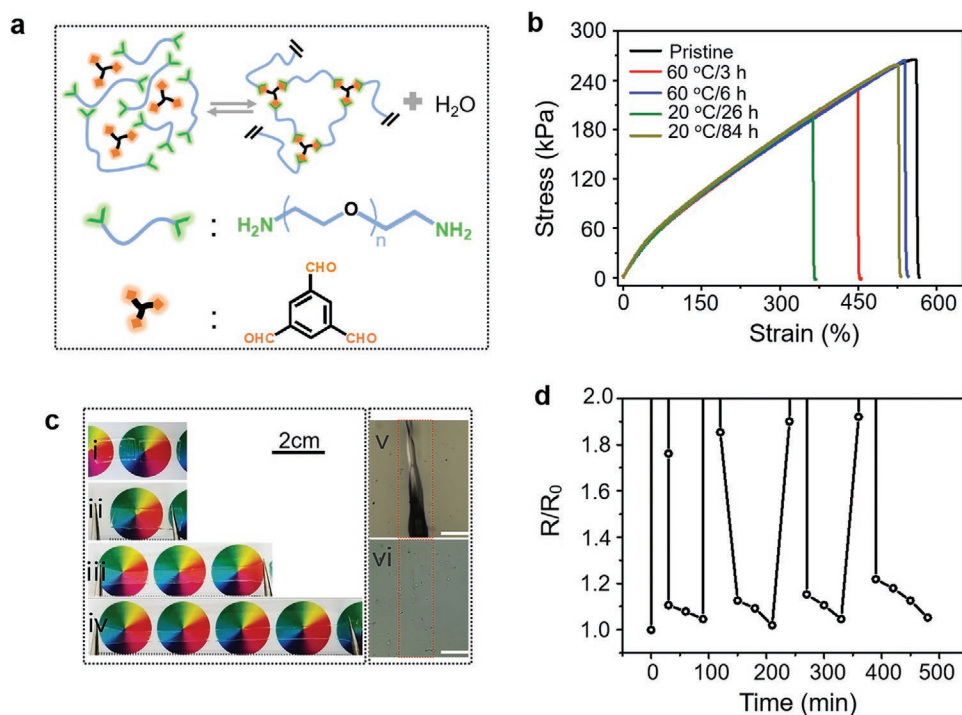


Figure 3. Self-healing property of the DC-PEO/LiTFSI. a) Self-healing mechanism of DC-PEO/LiTFSI. Bis(amine)-terminated PEO and 1,3,5-triformylbenzene form reversible imine bonds through a Schiff base reaction, which are cleaved upon damages and recovered after an autonomous healing process. b) The uniaxial tensile stress–strain profiles of DC-PEO/LiTFSI at pristine state and healed for different periods of time at RT (20 °C) and 60 °C after completely cutting into two pieces. c) Optical photos of DC-PEO/LiTFSI being cut (i), healed for 90 h at RT (ii), and stretched for different strains (iii,iv). Optical microscopy images of a cut DC-PEO/LiTFSI before (v) and after (vi) 48 h of healing at RT. Scale bar: 200 μm . d) Recovery of the resistance of the DC-PEO/LiTFSI after being completely cut and healed at 60 °C for several times.

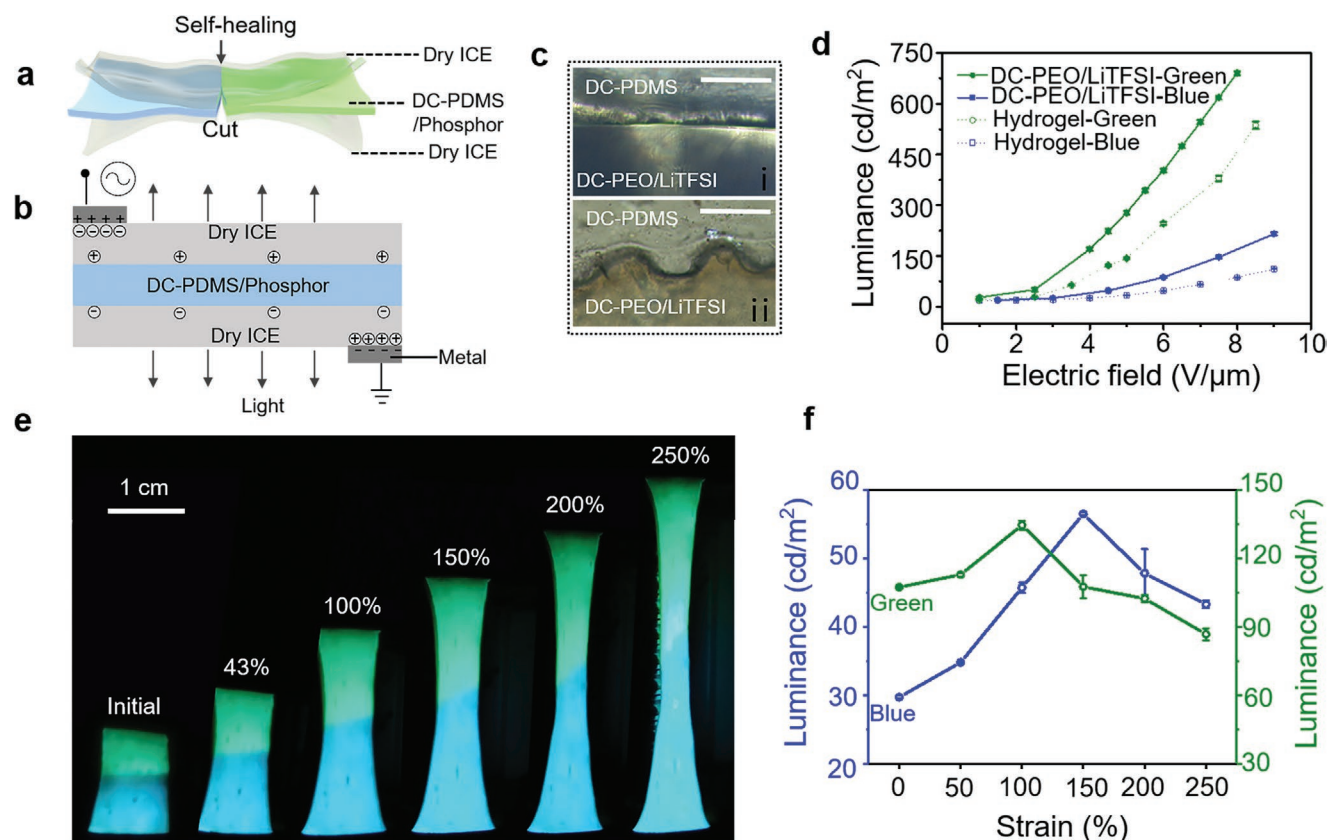


Figure 4. Iontronic AC electroluminescent (EL) devices. a) Schematic illustration of the EL device with three-layer sandwich structure. The entire device was intrinsically self-healable and highly stretchable. Both the DC-PDMS and DC-PEO/LiTFSI dry ICE are self-healable. b) The working principles for the EL device under an alternating voltage. c) The interface between the DC-PEO/LiTFSI and the DC-PDMS: i) freshly stacked together; ii) after 24 h. Scale bar: 200 μm . d) Luminance versus the applied fields at 2000 Hz frequency for green and blue EL device with the DC-PEO/LiTFSI and PAAm hydrogel as the electrode, respectively. e) Photographs showing the two-color healed EL device stretched to 250%, demonstrating simultaneously its self-healing capability and the stretchability. f) The corresponding luminance of the two-color healed EL device under different tensile strains.

has no corrosion to metals since it is solvent-free, but hydrogels could show corroding effect on metals.^[16,17]

An iontronic AC EL device was constructed using the DC-PEO/LiTFSI ICE as the two electrodes, as schematically shown in **Figure 4a**. The luminescent layer consists of dynamic crosslinking poly(dimethylsiloxane) (DC-PDMS) mixed with 67 wt% of phosphor particles. The DC-PDMS dielectric elastomer was also dynamically crosslinked with imine bonds, achieving also high stretchability and self-healing capability according to our previous work^[25] (Figure S9, Supporting Information). Therefore, the entire device was intrinsically self-healable and highly stretchable. The DC-PDMS is highly transparent ($\approx 96\%$ in the visible range); the DC-PEO/LiTFSI has a light yellowish color but still shows good transmittance of $\approx 78\%$ (both 200 μm thick) (Figure S10, Supporting Information). The light yellowish color is attributed to the oxidation of the amines in air, which changes to darker yellow after heat-treatment but changes to colorless transparent after the reduction by NaBH_3CN . The working principles for the EL device under an alternating voltage was shown in Figure 4b, where the AC electric field was applied on the luminescent layer through the electric double layer (EDL) at the metal wire/ICE interfaces.

The interface between the ionic electrode and the dielectric luminescent layer is a critical factor influencing the

performance of EL devices, both the mechanical robustness and the luminescent properties. The DC-PEO/LiTFSI and DC-PDMS can have relatively strong bonding at the interfaces. As shown in Figure 4c, their original clear interface becomes fuzzy after 24 h at RT. After sticking a piece of DC-PEO/LiTFSI to the DC-PDMS for 2 days at RT, the strong bonding at the interfaces was confirmed by the corresponding tensile profile (Figure S11, Supporting Information). This robust interface is an advantage over the hydrogel-based iontronic EL devices, where the hydrophobic dielectric layer has poor bonding with hydrophilic hydrogel electrode (Figure S12, Supporting Information). We compared the EL performances of our EL devices using the dry ICE electrode to that using a PAAm hydrogel electrode. EL devices with two kinds of phosphor particles were tested, glowing blue and green light respectively. For all samples, the luminance increases with the applied field (Figure 4d) and frequency, but achieve saturation after ≈ 2.5 kHz (Figure S13, Supporting Information), similar to previous reported trends.^[38] The luminance of the dry ICE-based EL device is higher than that of hydrogel-based device, though PAAm hydrogel has higher ionic conductivity (0.0235 S cm^{-1}). For example, the green-light luminance of dry ICE-based EL device reached 402 cd cm^{-2} at $6 \text{ V } \mu\text{m}^{-1}$ electric field, which is 64% higher than that using hydrogel electrode. The better EL property is

attributed to the better interface between the dry ICE electrode and luminescent layer. It is also worth mentioning that the dielectric constant k of DC-PDMS is slightly higher than that of commercial PDMS (Figure S14, Supporting Information), which leads to the higher luminous intensity than that of the EL device using the commercial PDMS in luminescent layer.^[38]

To demonstrate that the entire EL device was intrinsically self-healable and highly stretchable, we attached a green and a blue EL device together, healed the boundary at RT for 24 h, and then tested their luminance at stretched states. The two-color healed EL device can be stretched to 250%. At every stretched state, both the blue-color and green-color parts deformed evenly, confirming the fully recovery of the ionic electrodes and the luminescent layers at the boundary (Figure 4e). The corresponding luminance of both colors increases with strain at first, and then decreases with the strain (Figure 4f). The intensity variation trend can be explained by a combined effect of the increase in the emission area (i.e., lowered light-emitting particle density) and the decrease in thickness of the luminescent layer (i.e., larger electrical field). The latter effect dominates at small strain states, leading to the intensity increase; the former effect dominates at large strain states and reverses the trend. This trend of the healed two-color device is the same as the two separate devices emitting green light and blue light, respectively (Figure S15, Supporting Information).^[9]

The DC-PEO/LiTFSI can operate at relatively high temperature (as suggested by Figures 1c,d and 2a) and is long-term stable since it is dry. Its conductivity and weight remained almost the same after 16 h treatment at 80 °C (Figure 5a). After further storage at RT for 4 months, the conductivity and weight were still the same. In contrast, the conductivity of the counterpart PAAm hydrogel decreased drastically to only $\approx 5\%$ of that before treatment and its weight also kept decreasing during

the 16 h treatment at 80 °C. As for the mechanical properties, the tensile strength decreased slightly while the fracture strain remained almost the same after 80 °C treatment and 4 months storage at RT (Figure 5b). In contrast, the counterpart PAAm hydrogel changed from elastomer to brittle plastics without stretchability after the 80 °C treatment (Figure S16, Supporting Information). The deterioration of the hydrogel performances is due to the evaporation of the water at high temperature (as suggested by TGA data in Figure S17, Supporting Information).

The stability of the dry ICE electrode ensures the stability of the EL device. The luminance of a flower-shaped dry ICE-based EL device decreased slightly from 235 to 205 cd m^{-2} after 16 h at 80 °C (Figure 5d). On the contrary, luminance of a counterpart hydrogel-based device decreased from 143.5 to 64.9 cd m^{-2} after 16 h treatment at 80 °C. Meantime, the size and shape of the dry device remained the same throughout the course of treatment; while the hydrogel-based device shrunk significantly and became brittle after the treatment (Figure 5c and Figures S16 and S12: Supporting Information). The dry EL device also showed stable luminescent property over 9 weeks' storage at ambient environment (Figure S18, Supporting Information). These results strongly support the excellent stability and wide temperature range of the dry ICE and corresponding devices, due to the elimination of solvent evaporation issue.

An iontronic TENG (iTENG) was also demonstrated for tactile sensor using the DC-PEO/LiTFSI as electrode and DC-PDMS as electrification layer, as shown in Figure 6a. This iTENG sensor overall was also intrinsically self-healable and stretchable. The iTENG is grounded through an external resistor, so it works in the single-electrode mode (Figure 6b).^[3] When a hand contacts with the DC-PDMS dielectric layer, electrification happens at the interface, generating the same

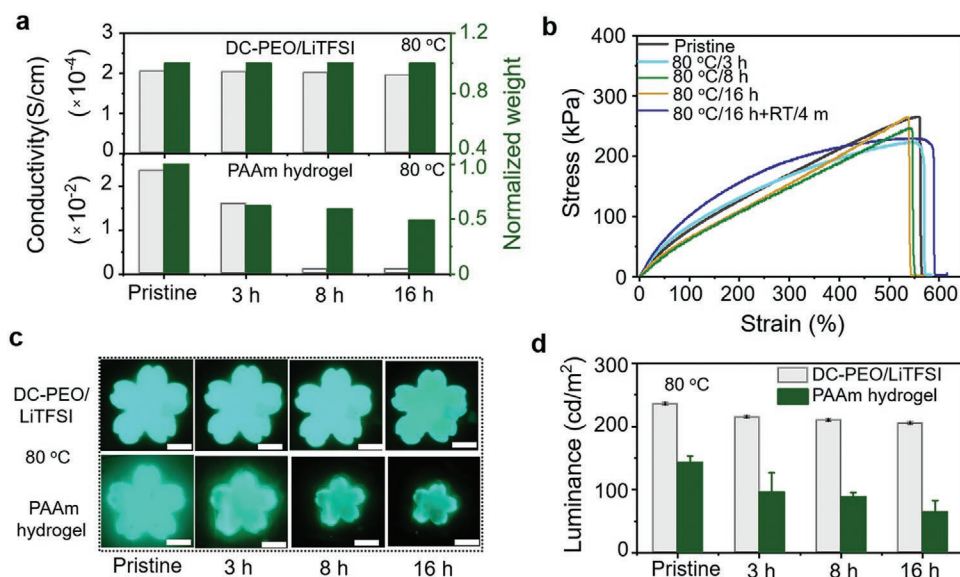


Figure 5. Stability of the DC-PEO/LiTFSI dry ICE and the iontronic EL devices. a) The conductivity and weight of DC-PEO/LiTFSI dry ICE and PAAm hydrogel after different heat treatments. b) The tensile profiles of DC-PEO/LiTFSI after different heat treatments. c) Photographs of the two blue flower EL devices stored at 80 °C for different times. The upside is the EL device with DC-PEO/LiTFSI as the electrode, the downside is the EL device with PAAm hydrogel as the electrode. Scale bar: 5 mm. The EL devices were all illuminated at the applied field of $5 \text{ V } \mu\text{m}^{-1}$ and the frequency of 2000 Hz. The thickness of DC-PDMS dielectric layer was 200 μm . d) The corresponding luminance of the dry ICE-based and hydrogel-based EL devices after treated at 80 °C for different times. The measurements obtained from this work were reproduced with three samples for each condition.

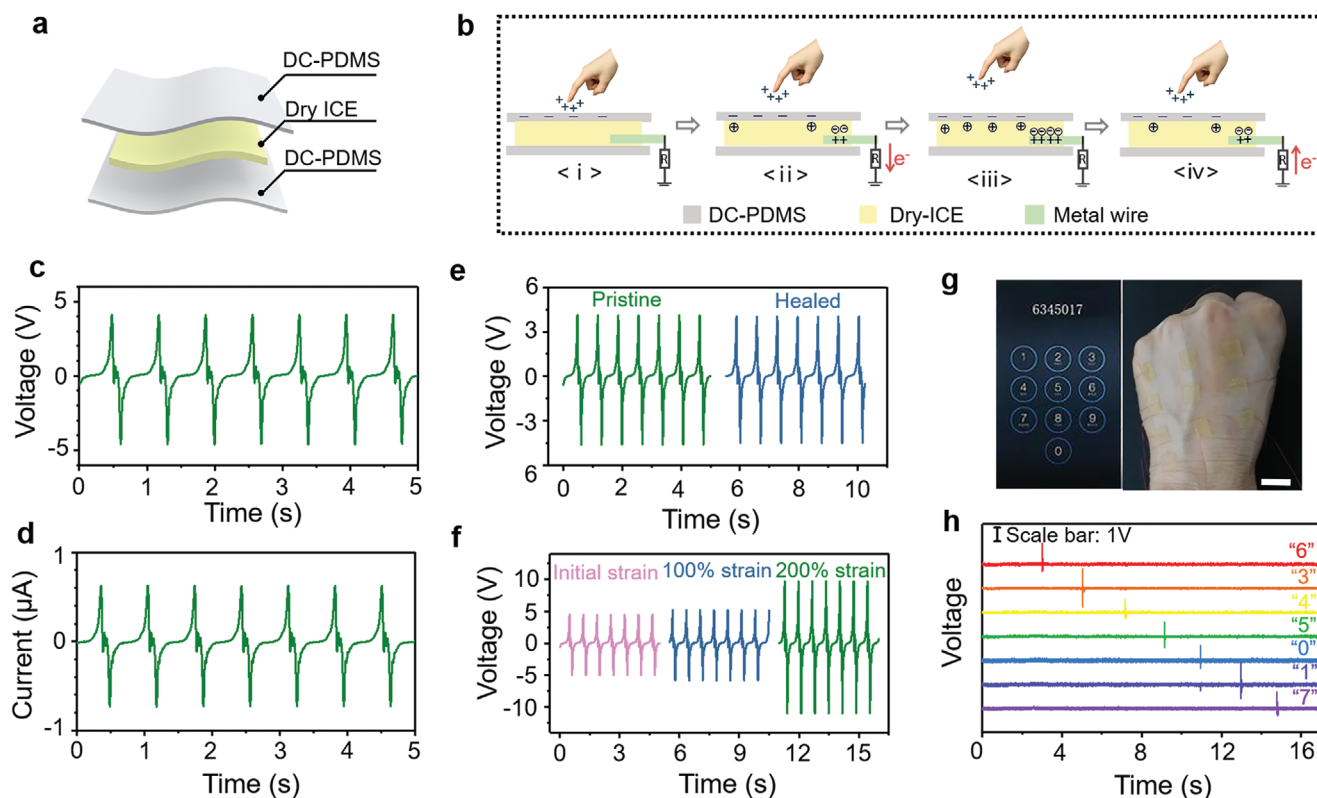


Figure 6. Iontronic triboelectric nanogenerator (iTENG) tactile sensors. a) Schematic illustration of the architecture for an iTENG. The entire device was intrinsically self-healable and highly stretchable. b) The working principles for iTENG at single-electrode mode. c,d) The output voltage (c) and current (d) of an iTENG connected to the ground through a 1.2 M Ω resistor. e) The voltage of an iTENG before and after healing the damages, and f) at different tensile strains. g) Image of a touch panel keyboard with 10 iTENG tactile sensors attached on a curvy hand. Scale bar: 1 cm. h) Voltage profiles of the channels of touched digits.

amount of electrostatic charges with opposite polarities at the fingertip and the DC-PDMS, respectively (Figure 6b-i). When the hand is moving away, the static charges in DC-PDMS will induce the formation of a layer of excessive ions at the interface of DC-PEO/LiTFSI and DC-PDMS to balance the static charges (Figure 6b-ii). Meanwhile, an electrical double layer is formed at the interface of the DC-PEO/LiTFSI and metal wire tip, resulting in the electron flux from the metal wires to the ground until all the static charges in the DC-PDMS are screened (Figure 6b-iii). When the hand is approaching back, an electron flux with the opposite direction will transfer through the external resistor (Figure 6b-iv). If the relative contact-separation motion is repeated, pulsed AC current will be generated continuously.^[39,40]

We first characterized the output of the iTENG at open-circuit and short-circuit condition respectively, with a latex film to carry out the contact-separation motion (area, 3 \times 3 cm²) (Figure S19, Supporting Information). The peak open-circuit voltage V_{oc} and the peak short-circuit charge Q_{sc} are about 120 V and 40 nC, respectively. The peak-to-peak value of short-circuit current I_{sc} was measured to be \approx 1.9 μ A. The iTENG featured as a current source with high internal impedance. Therefore, the current showed no significant decrease until the external resistance reached 100 M Ω scale, and a maximum areal power density of \approx 127 mW m⁻² was achieved at a matched resistance of \approx 512 M Ω .

As for the application as a tactile sensor, a 1.2 M Ω resistor was connected to an iTENG, so as to lower the measured voltage for the convenience of signal acquisition. The voltage drop across the resistor had a peak-to-peak value of \approx 8.8 V, while the peak-to-peak current value was \approx 1.37 μ A (Figure 6c,d). To evaluate the self-healing ability, the iTENG sensor was cut in the middle by a razor blade, attached back, and then healed spontaneously at ambient conditions for 24 h. The voltage of healed iTENG showed no significant drop, suggesting the recovery of both the DC-PEO/LiTFSI electrode and the DC-PDMS dielectric layers (Figure 6e). The stretchability of the iTENG sensor was further examined. The voltage increased at stretched state due to the increase in contact area and decrease in thickness of the electrification layer (Figure 6f), which is consistent with previous reported observations.^[9]

The soft and transparent iTENG can be applied as an artificial-skin-like touch panel. 10 iTENG sensors were fabricated in one panel with each correspondent to one of the 10 digits. This soft panel can be conformally attached onto a curvy hand (Figure 6g), and be able to perceive the touch by alien objects and to function as a touch keyboard. A multichannel measurement system was used to simultaneously obtain the electric signals from all the iTENG sensors. For demonstration, a series of numbers “6 345 017” were generated by pressing the panel with a finger, and the corresponding electrical signals were shown in Figure 6h.

3. Conclusion

We have demonstrated an effective approach to improve the ionic conductivity of dry ion-conducting elastomers, and simultaneously achieved self-healing capability, stretchability and transparency. Due to the elimination of liquid leakage or evaporation issues suffered by state-of-the-art ion-conducting gels, this ionic conductor showed wide operational temperature range and relatively great thermal stability. These advantageous properties made it highly promising for multifunctional stretchable/soft iontronics or electronics, as exemplified by but not restricted to the EL devices and TENG sensors in this work. Furthermore, this dynamic crosslinking strategy can be applied to other dry ion-conducting polymer electrolyte materials other than PEO derivatives, so as to promote their applications in multifunctional iontronics/electronics. Lastly, this strategy is also helpful for solid-state electrochemical energy devices, where high ionic conductivity and thermal stability are still long-lasting pursuits for solid electrolytes. Therefore, our findings not only demonstrate the soft iontronics with dry ICE electrodes, but also develop a general strategy for high-performance solid polymer electrolytes.

4. Experimental Section

Materials: Poly(ethylene oxide) (PEO) (Macklin, $M_w = 100\,000\text{ g mol}^{-1}$), poly(ethylene oxide) bis(amine) ($\text{H}_2\text{N-PEO-NH}_2$) ($M_w = 2000\text{ g mol}^{-1}$, Aladdin), benzene-1,3,5-tricarbaldehyde (Ark Pharm), bis(amine)-terminated poly(dimethylsiloxane) ($\text{H}_2\text{N-PDMS-NH}_2$) ($M_n = 5000\text{ g mol}^{-1}$, Gelest DMS-A21), lithium bis(trifluoromethane sulfonamide) (LiTFSI) (Macklin), *N,N*-dimethylformamide (DMF) (Macklin), acetonitrile (Macklin), and dichloromethane (Macklin) were all used as received. Zinc sulfide (ZnS) phosphor powders doped with different transition metal elements to luminesce in green color and blue color (Shandong Wanji High-tech Electronics Co. Ltd., Shandong, China) were used as received.

Fabrication of the Dynamic Crosslinking DC-PEO/LiTFSI, L-PEO/LiTFSI, and C-PEO/LiTFSI: In this study, the ratio of EO: Li was 8:1. DC-PEO/LiTFSI was synthesized by mixing 400 mg of $\text{H}_2\text{N-PEO-NH}_2$ and 2 mL DMF solution with 26 mg 1,3,5-triformylbenzene and 0.328 g LiTFSI in it. The mixture was transferred to a poly(tetrafluoroethylene) (PTFE) molded container. A gel was obtained at first. To remove the solvent in the gel, the sample was stored in the oven at 60 °C for 48 h to get a dry DC-PEO/LiTFSI elastomer. To contrast, the L-PEO/LiTFSI ($M_w = 100\,000\text{ g mol}^{-1}$) were also prepared. The methods were as follows: First, mix PEO powder with LiTFSI in the ziplock bag. The ratio of EO: Li was also 8:1. Then, mix them in a Banbury mixer at 140 °C for 4 min to obtain dry L-PEO/LiTFSI.

The reductive amination of DC-PEO was prepared as follows: at first, mix 400 mg of $\text{H}_2\text{N-PEO-NH}_2$ and 2 mL DMF solution with 26 mg 1,3,5-triformylbenzene and 0.328 g LiTFSI in it. Wait for 40 min at room temperature to get an imine gel. Then, adjust the pH to 6 with acetic acid and dissolve 16.8 mg NaBH_3CN into the mixture. Lastly, remove the air bubbles with ultrasonic water bath and transfer the solution into a PTFE mode and treat it in an oven at 60 °C for 72 h in the vacuum oven to obtain the reductive amination of DC-PEO, which is the crosslinking PEO (C-PEO/LiTFSI).

Fabrication of the Dynamic Crosslinking PDMS (DC-PDMS): DC-PDMS was synthesized by mixing 2 g of $\text{H}_2\text{N-PDMS-NH}_2$ and 300 μL dichloromethane solution with 33 mg 1,3,5-triformylbenzene in it. The viscosity of the solution increased drastically in several minutes. The mixture was dried in a PTFE container at room temperature for 12 h and then heated to 80 °C for 5 h. Dynamic imine bonds were formed, and the PDMS chains were dynamically crosslinked to generate the transparent

and healable elastomer. The DC-PDMS elastomer can be pressed into a film with any thickness using a mold at 80 °C.

Fabrication of the PAAM-LiCl Hydrogel: According to a previous report,^[3] add acrylamide into 4 M LiCl aqueous solution. The concentration of acrylamide to deionized water was fixed at 14 wt%. Secondly, add *N,N'*-methylenebisacrylamide, ammonium persulfate, and *N,N,N',N'*-tetramethylethylenediamine into the solution. Thirdly, transfer the solution into a plastic culture dish and treat it in an oven at 50 °C for 2 h to form the PAAM-LiCl hydrogel. The thickness of the final hydrogel is around 2 mm.

Fabrication of the Iontronic Electroluminescent (EL) Device: DC-PDMS was used as the dielectric layer matrix of the self-healing EL device. The weight ratio of the ZnS phosphor powders to DC-PDMS was 2:1. At first, 2 g of bis(amine)-terminated poly(dimethylsiloxane) and 4 g ZnS phosphor powders (blue or green) were dissolved in 2 mL dichloromethane solution. Then 33 mg 1,3,5-triformylbenzene was added into the mixture. Before the viscosity of the solutions increased, transfer the mixture into a PTFE container at room temperature for 1 h and then heated to 80 °C for 5 h to evaporate the dichloromethane solution totally. The healable dielectric layer DC-PDMS/ZnS elastomer was hot pressed at 80 °C with a 200 μm -thickness mold. The self-healing EL device was fabricated by sandwiching the dielectric layer DC-PDMS/ZnS composites between two DC-PEO/LiTFSI layers. PEN/ITO electrode and aluminum tape were used to electrically connect the electrode with the external power source.

Fabrication of the Iontronic TENG and Tactile Sensor: The iTENG was fabricated by sandwiching DC-PEO/LiTFSI between two dielectric DC-PDMS layers. Aluminum tape and copper wire were used to electrically connect the electrode with the external load.

Materials Characterization: FTIR-ATR measurements were performed on a VERTEX 80v spectrometer (Bruker) from 600 to 4000 cm^{-1} . The mechanical tensile test, stretch cycling test and peeling test were all conducted by an ESM301/Mark-10 system. The strain rate was fixed at 30, 60, and 60 mm min^{-1} , respectively. The peeling test was conducted using samples with the size of 0.6 mm (thickness) \times 1 cm (width) \times 4 cm (length) each. The samples were sandwiched between two same materials. The tests were conducted at room temperature immediately after the two surfaces attached to each other. All the tests above were conducted at room temperature. The optical transmittance was measured by a Shimadzu UV-3600 spectrophotometer. The impedance tests were performed on an electrochemical workstation (CHI660E), and the samples were sandwiched by two stainless steel electrode for tests. Differential scanning calorimetry measurement (DSC) was performed on DSC 200F3 (NETZSCH) in N_2 atmosphere. Liquid nitrogen was used to decrease the temperature. The temperature was increased from -80 to 300 °C at the rate of 10 °C min^{-1} . Thermogravimetric analysis (TGA) was performed on TGA5500 (TA instruments) in N_2 atmosphere. The heating rate was also 10 °C min^{-1} . X-ray diffraction (XRD) measurements were carried out using benchtop Proto AXRD system (Cu $K\alpha$, $\lambda = 0.154\text{ nm}$) in the 2θ range of 10°–50°. The dielectric constant was measured by the LCR meter (KEYSIGHT, E4980A) from 1 Hz to 1 MHz.

EL Device Characterization: Alternating voltage signals (standard sine wave) for activating LECs were generated using NI-cDAQ 9138 programmed through a custom script. The signals were amplified by a high voltage amplifier (Trek 610E), where the V values reported are the peak voltages of the sine wave. The luminance values were measured by a luminance meter (TOPCON BM-7) placed at a perpendicular distance of 30 mm from the center of the samples.

iTENG and Touch Panels Characterization: A step motor (LinMot E1100) was used to provide the input of mechanical motions. For all the tests of energy generation of the iTENG, the pressure (100 kPa), speed (2 m s^{-1}), and frequency ($\approx 2\text{ Hz}$) of the step motor were fixed. The humidity was around 10%. The voltage, charge and current quantity were recorded by a Keithley electrometer 6514. The force applied by the motor was detected by a Mark-10 force gauge. A multichannel measurement system (PXIe 4300, National Instruments Corporation) was used to simultaneously obtain the electric signals from all the 10 electrode lines from the touch panels.

DFT Calculations: DFT calculations were performed in the Vienna ab initio Simulation Package (VASP).^[41] The projector augmented wave (PAW)^[42] method with the Perdew–Burke–Ernzerhof (PBE) exchange–correlation functional^[43] were used in all calculations. To simplify the calculation, 5 EO repeat units were just used for the PEO chain. The plane-wave basis kinetic energy cut-off was set to 400 eV. For the geometry optimization of DC-PEO/LiTFSI molecule, all atoms were allowed to be relaxed until the forces were less than 0.05 eV Å⁻¹. Then with the optimized DC-PEO/LiTFSI molecule, the adsorption behaviors of Li⁺ ions on the DC-PEO/LiTFSI molecule were estimated by binding energy calculation. The binding energy of a Li⁺ ion on the DC-PEO/LiTFSI molecule was defined by the following equation:

$$E_{\text{ad}} = E_{\text{mol-Li}} - E_{\text{mol}} - E_{\text{Li}} \quad (1)$$

where $E_{\text{mol-Li}}$ and E_{mol} are the energies of the DC-PEO/LiTFSI molecule adsorbing a Li⁺ ion and without adsorption. Here, E_{Li} is the energy of an isolated Li atom. During the relaxation of Li⁺ ion adsorbed DC-PEO/LiTFSI molecule, the Li⁺ ion and atoms of DC-PEO/LiTFSI with the distances away from Li atom less than 6 Å were allowed to relax until the forces on all the relaxed atoms were less than 0.05 eV Å⁻¹.

Supporting Information

Supporting Information is available from the Wiley Online Library or from the author.

Acknowledgements

The authors thank for the support from the Youth Innovation Promotion Association of CAS (2017055), National Key Research and Development Program of China (2016YFA0202702 and 2017YFB0702100), Youth Backbone Individual Project of Beijing Excellent Talents Training (Y9QNGG2701). The authors thank for the help from Prof. Yadong Lv and Prof. Jiangman Sun. No formal ethical approval was required for the demonstration in Figure 6g; the attachment of this device on the hand is not harmful and was consented by the volunteer.

Conflict of Interest

The authors declare no conflict of interest.

Data Availability Statement

Research data are not shared.

Keywords

electroluminescent devices, ion-conducting elastomers, iontronics, self-healing, triboelectric nanogenerators

Received: February 18, 2021

Revised: April 9, 2021

Published online:

[1] H. J. Kim, B. Chen, Z. Suo, R. C. Hayward, *Science* **2020**, 367, 773.

[2] C. Yang, Z. Suo, *Nat. Rev. Mater.* **2018**, 3, 125.

[3] X. Pu, M. Liu, X. Chen, J. Sun, C. Du, Y. Zhang, J. Zhai, W. Hu, Z. L. Wang, *Sci. Adv.* **2017**, 3, 1700015.

[4] H. Chun, T. D. Chung, *Annu. Rev. Anal. Chem.* **2015**, 8, 441.

[5] H. R. Lee, C. C. Kim, J. Y. Sun, *Adv. Mater.* **2018**, 30, 1704403.

[6] C. Keplinger, J.-Y. Sun, C. C. Foo, P. Rothmund, G. M. Whitesides, Z. Suo, *Science* **2013**, 341, 984.

[7] P. Brochu, Q. Pei, *Macromol. Rapid Commun.* **2010**, 31, 10.

[8] C. H. Yang, B. Chen, J. J. Lu, J. H. Yang, J. Zhou, Y. M. Chen, Z. Suo, *Extreme Mech. Lett.* **2015**, 3, 59.

[9] J. Wang, C. Yan, G. Cai, M. Cui, A. L. S. Eh, P. S. Lee, *Adv. Mater.* **2016**, 28, 4490.

[10] J. Wang, C. Yan, K. J. Chee, P. S. Lee, *Adv. Mater.* **2015**, 27, 2876.

[11] C. H. Yang, S. Zhou, S. Shian, D. R. Clarke, Z. Suo, *Mater. Horiz.* **2017**, 4, 1102.

[12] C. C. Kim, H. H. Lee, K. H. Oh, J. Y. Sun, *Science* **2016**, 353, 682.

[13] K. Parida, V. Kumar, J. X. Wang, V. Bhavanasi, R. Bendi, P. S. Lee, *Adv. Mater.* **2017**, 29, 1702181.

[14] P. Calvert, *Adv. Mater.* **2009**, 21, 743.

[15] P. Zhang, Y. Chen, Z. H. Guo, W. Guo, X. Pu, Z. L. Wang, *Adv. Funct. Mater.* **2020**, 30, 1909252.

[16] L. Shi, T. Zhu, G. Gao, X. Zhang, W. Wei, W. Liu, S. Ding, *Nat. Commun.* **2018**, 9, 2630.

[17] X. Qu, W. Niu, R. Wang, Z. Li, Y. Guo, X. Liu, J. Sun, *Mater. Horiz.* **2020**, 7, 2994.

[18] B. Yiming, Y. Han, Z. Han, X. Zhang, Y. Li, W. Lian, M. Zhang, J. Yin, T. Sun, Z. Wu, T. Li, J. Fu, Z. Jia, S. Qu, *Adv. Mater.* **2021**, 33, 2006111.

[19] B. B. Jing, C. M. Evans, *J. Am. Chem. Soc.* **2019**, 141, 18932.

[20] Z. Xue, D. He, X. Xie, *J. Mater. Chem. A* **2015**, 3, 19218.

[21] Z. Gadjourova, Y. G. Andreev, D. P. Tunstall, P. G. Bruce, *Nature* **2001**, 412, 520.

[22] P. Johansson, *Polymer* **2001**, 42, 4367.

[23] S. K. Fullerton-Shirey, J. K. Maranas, *Macromolecules* **2009**, 42, 2142.

[24] X. Yu, J. Li, A. Manthiram, *ACS Mater. Lett.* **2020**, 2, 317.

[25] J. Sun, X. Pu, M. Liu, A. Yu, C. Du, J. Zhai, W. Hu, Z. L. Wang, *ACS Nano* **2018**, 12, 6147.

[26] J. F. Zhang, D. Z. Yang, F. Xu, Z. P. Zhang, R. X. Yin, J. Nie, *Macromolecules* **2009**, 42, 5278.

[27] Y. Li, Z. Sun, D. Liu, Y. Gao, Y. Wang, H. Bu, M. Li, Y. Zhang, G. Gao, S. Ding, *J. Mater. Chem. A* **2020**, 8, 2021.

[28] R. Uchiyama, K. Kusagawa, K. Hanai, N. Imanishi, A. Hirano, Y. Takeda, *Solid State Ionics* **2009**, 180, 205.

[29] K. Y. Cho, K. H. Lee, J. K. Park, *Polym. J.* **2000**, 32, 537.

[30] R. Khurana, J. L. Schaefer, L. A. Archer, G. W. Coates, *J. Am. Chem. Soc.* **2014**, 136, 7395.

[31] J. Y. Wan, J. Xie, X. Kong, Z. Liu, K. Liu, F. F. Shi, A. Pei, H. Chen, W. Chen, J. Chen, X. K. Zhang, L. Q. Zong, J. Y. Wang, L. Q. Chen, J. Qin, Y. Cui, *Nat. Nanotechnol.* **2019**, 14, 705.

[32] N. Wu, Y. R. Shi, S. Y. Lang, J. M. Zhou, J. Y. Liang, W. Wang, S. J. Tan, Y. X. Yin, R. Wen, Y. G. Guo, *Angew. Chem., Int. Ed.* **2019**, 58, 18146.

[33] Z. Huang, Q. Pan, D. M. Smith, C. Y. Li, *Adv. Mater. Interfaces* **2019**, 6, 1801445.

[34] D. Lin, W. Liu, Y. Liu, H. R. Lee, P.-C. Hsu, K. Liu, Y. Cui, *Nano Lett.* **2016**, 16, 459.

[35] D. G. Mackanic, X. Yan, Q. Zhang, N. Matsuhisa, Z. Yu, Y. Jiang, T. Manika, J. Lopez, H. Yan, K. Liu, X. Chen, Y. Cui, Z. Bao, *Nat. Commun.* **2019**, 10, 5384.

[36] A. Chao, J. Negulescu, D. Zhang, *Macromolecules* **2016**, 49, 6277.

[37] M. E. Belowich, J. F. Stoddart, *Chem. Soc. Rev.* **2012**, 41, 2003.

[38] Y. J. Tan, H. Godaba, G. Chen, S. T. M. Tan, G. Wan, G. Li, P. M. Lee, Y. Cai, S. Li, R. F. Shepherd, J. S. Ho, B. C. K. Tee, *Nat. Mater.* **2020**, 19, 182.

[39] Z. L. Wang, *Adv. Energy Mater.* **2020**, 10, 2000137.

[40] Z. L. Wang, *Mater. Today* **2017**, 20, 74.

[41] G. Kresse, J. Furthmüller, *Phys. Rev. B* **1996**, 54, 11169.

[42] P. E. Blochl, *Phys. Rev. B* **1994**, 50, 17953.

- [43] J. P. Perdew, K. Burke, M. Ernzerhof, *Phys. Rev. Lett.* **1996**, *77*, 3865.
- [44] Z. Wang, S. Wang, A. Wang, X. Liu, J. Chen, Q. Zeng, L. Zhang, W. Liu, L. Zhang, *J. Mater. Chem. A* **2018**, *6*, 17227.
- [45] W. J. Tang, S. Tang, C. J. Zhang, Q. T. Ma, Q. Xiang, Y. W. Yang, J. Y. Luo, *Adv. Energy Mater.* **2018**, *8*, 1800866.
- [46] D. G. Mackanic, W. Michaels, M. Lee, D. Feng, J. Lopez, J. Qin, Y. Cui, Z. Bao, *Adv. Energy Mater.* **2018**, *8*, 1800703.
- [47] J. Zhang, J. Zhao, L. Yue, Q. Wang, J. Chai, Z. Liu, X. Zhou, H. Li, Y. Guo, G. Cui, L. Chen, *Adv. Energy Mater.* **2015**, *5*, 1501082.
- [48] D. Zhou, Y. B. He, R. Liu, M. Liu, H. Du, B. Li, Q. Cai, Q.-H. Yang, F. Kang, *Adv. Energy Mater.* **2015**, *5*, 1500353.
- [49] C. Zuo, M. Yang, Z. Wang, K. Jiang, S. Li, W. Luo, D. He, C. Liu, X. Xie, Z. Xue, *J. Mater. Chem. A* **2019**, *7*, 18871.
- [50] Z. Sun, Y. Li, S. Zhang, L. Shi, H. Wu, H. Bu, S. Ding, *J. Mater. Chem. A* **2019**, *7*, 11069.
- [51] C. Niu, J. Liu, G. Chen, C. Liu, T. Qian, J. Zhang, B. Cao, W. Shang, Y. Chen, J. Han, J. Du, Y. Chen, *J. Power Sources* **2019**, *417*, 70.
- [52] G. Luo, B. Yuan, T. Guan, F. Cheng, W. Zhang, J. Chen, *ACS Appl. Energy Mater.* **2019**, *2*, 3028.
- [53] C. Cao, Y. Li, S. Chen, C. Peng, Z. Li, L. Tang, Y. Feng, W. Feng, *ACS Appl. Mater. Interfaces* **2019**, *11*, 35683.